Engineering 5 (2019) 880–887

Contents lists available at ScienceDirect

Engineering

journal homepage: www.elsevier.com/locate/eng

Research
Water Pollution Control—Article

Green Synthesis of Magnetic Adsorbent Using Groundwater Treatment Sludge for Tetracycline Adsorption

Zhan Qu [a,b], Yaqiong Wu [a], Suiyi Zhu [a,c,*], Yang Yu [d], Mingxin Huo [a], Leilei Zhang [a,*], Jiakuan Yang [b], Dejun Bian [a,c], Yi Wang [a]

[a] Science and Technology Innovation Center for Municipal Wastewater Treatment and Water Quality Protection, Northeast Normal University, Changchun 130117, China
[b] School of Environmental Science and Engineering, Huazhong University of Science and Technology, Wuhan 430074, China
[c] Engineering Lab for Water Pollution Control and Resources Recovery, Northeast Normal University, Changchun 130117, China
[d] Guangdong Shouhui Lantian Engineering and Technology Corporation, Guangzhou 510075, China

ARTICLE INFO

Article history:
Received 5 November 2018
Revised 27 January 2019
Accepted 7 March 2019
Available online 22 June 2019

Keywords:
Groundwater treatment sludge
Maghemite
Cationic exchange
Adsorption
Tetracycline

ABSTRACT

Groundwater treatment sludge is an industrial waste that is massively produced from groundwater treatment plants. Conventional methods for treatment of this sludge, such as discharge into deep wells or the sea, or disposal at landfills, are not environmentally sustainable. Here, we demonstrate an alternative strategy to recycle the sludge by preparing a magnetic maghemite adsorbent via a one-step hydrothermal method with NaOH solution as the only solvent. With this method, the weakly magnetized sludge, which contained 33.2% iron (Fe) and other impurities (e.g., silicon (Si), aluminum (Al), and manganese (Mn)), was converted to magnetic adsorbent (MA) with the dissolution of Si/Al oxides (e.g., quartz and albite) into the liquid fraction. At a NaOH concentration of 2 mol·L^{-1}, approximately 18.1% of the ferrihydrite in the Fe oxides of the sludge was converted into 11.2% maghemite and 6.9% hematite after the hydrothermal treatment. MA2 (i.e., MA produced by a 2 mol·L^{-1} NaOH concentration) exhibited a good magnetic response of 8.2 emu·g^{-1} (1 emu = 10^{-3} A·m^2), and a desirable surface site concentration of 0.75 mmol·g^{-1}. The synthesized MA2 was used to adsorb the cationic pollutant tetracycline (TC). The adsorption kinetics of TC onto MA2 fitted well with a pseudo-second-order model, and the adsorption isotherms complied well with the Langmuir model. The maximum adsorption capacity of MA2 for TC was 362.3 mg·g^{-1}, and the main mechanism for TC adsorption was cationic exchange. This study is the first to demonstrate the preparation of an MA from recycled sludge without a reductant and/or exogenous Fe source. The prepared adsorbent can be used as a low-cost adsorbent with high capacity for TC sorption in the treatment of TC-containing wastewater.

1. Introduction

Groundwater treatment sludge is an iron (Fe)-containing waste from groundwater treatment plants that is produced in large quantities as a waste product of potable water production [1,2]. The sludge contains fine particles and is rich in Fe and manganese (Mn) oxides [3]. Traditionally, the sludge is disposed of as waste by discharging it into deep wells and/or waterways, which may lead to the run-off of Fe/Mn into nearby waters [4]. Given tightening solid waste disposal regulations, groundwater treatment plants generally handle the sludge by mechanical dewatering and harmless solidification before sending it to landfills. However, this process is costly and complicated [5].

Recycling of Fe and Mn from the sludge is an optional strategy, but the addition of exogenous acid and Mn reagent [6,7] limits its application. In recent years, the sludge has been directly applied to adsorb phosphate and heavy metals, such as Ni^{2+} [7], Cu^{2+}, Zn^{2+}, and Cd^{2+} [8], in wastewater. After adsorption, the multistep separation process of the sludge from water includes tedious centrifugation, coagulation, and/or filtration [4,8]. Conversion of the weakly magnetized sludge into magnetic adsorbent (MA) may be an alternative option to rapidly separate the sludge from water.

Fe oxides in the sludge can be converted to magnetite by heating over 600 °C with the addition of coal [9] and iron(II) sulfide

* Corresponding authors.
E-mail addresses: papermanuscript@126.com (S. Zhu), zhangll554@nenu.edu.cn (L. Zhang).

https://doi.org/10.1016/j.eng.2019.06.001

(FeS), or the injection of hydrogen (H_2) [10] and methane (CH_4) [11]. The conversion can also be performed under a mild temperature of 160 °C via a facile hydrothermal method with ethylene glycol [3] or ascorbic acid [5] as a reductant. With the addition of reductant, the Fe^{3+} in the sludge is reductively dissolved into Fe^{2+} and then reoxidized to form magnetite and/or maghemite under different conditions [3]. Without the addition of reductant, the reductive dissolution of Fe oxides is interrupted [5,6]. As a result, the product is weakly magnetized.

A synthesized low-cost adsorbent produced from waste, with a good magnetic response [12], has been shown to have promising application in wastewater treatment [13]. The surface functional group (≡Fe–O–H) of the MA exhibited good adsorption capacities for both cationic and anionic contaminants in wastewater [14–16], especially for heavy metals and negatively charged colloid. In addition, the MA can be applied to the synthesis of carbon and/or silicon material [17,18] to enhance their magnetic separation after use [19,20].

This study reports the development of a new approach to convert sludge to MA without the addition of reductant. The capacity of the synthesized adsorbent is evaluated by adsorption of the positively charged contaminant tetracycline (TC).

2. Materials and method

2.1. Groundwater treatment sludge

Groundwater treatment sludge was acquired from a drinking water treatment plant in Panshi City in Jilin Province, China. The sludge was vacuum dried at 50 °C overnight and then subjected to wet chemical analysis following the method of Sandroni and Smith [21]. The major elements of the sludge based on the dry weight were Fe (33.2%), silicon (Si, 6.2%), Mn (4.9%), calcium (Ca, 2.1%), aluminum (Al, 1.4%), potassium (K, 0.3%), and magnesium (Mg, 0.2%).

2.2. Synthesis of magnetic adsorbent

The synthesis of the MA from the groundwater treatment sludge was conducted as follows: 1 g of dried sludge, 20 mL of deionized water, and 10 mL of NaOH solution were placed in a 50 mL conical flask and stirred at 250 $r \cdot min^{-1}$ for 5 min, and then transferred into a 50 mL Teflon kettle. The kettle was heated at 160 °C for 10 h and then cooled to room temperature. The precipitate was collected and removed from the kettle by a magnet and then washed five times with deionized water, followed by vacuum drying overnight. In the experiment, the concentration of the NaOH solution was variably set at 0.6, 1, 2, and 4 $mol \cdot L^{-1}$, respectively, and the obtained MAs were denoted as "MA*x*" (where *x* represents the NaOH concentration).

2.3. Characterization of adsorbent

The X-ray powder diffraction (XRD) patterns of the sludge and MA were determined using a diffractometry system (RAPID-S; Rigaku, Japan) with copper (Cu) Kα radiation in the 2θ range of 20°–50°. The crystalline phase of the Fe oxides in the sludge and MA was investigated with a transmission Mössbauer spectrometer (MS-500; Oxford Instruments, UK) at room temperature. Magnetic measurement was carried out at room temperature by magnetometry (SQUID-VSM; Quantum Design, USA) with a SQUID-VSM system. The composition of the MA was determined following the method of the sludge described in Section 2.1. The valence states of Mn on the sludge and MA surface were determined by X-ray photoelectron spectrometry (XPS, VG-ADES; Thermal VG, UK) with Mg Kα radiation. The morphologies of the sludge and of the MA were recorded by scanning electron microscopy (SEM, NanoSEM 450; FEI Co., USA).

2.4. Titration experiment

The total surface site concentrations (H_s) of the MA were determined by a potentiometric titration method [5]. First, 0.2 g of MA was added to 50 mL deionized water and then suspended by nitrogen (N_2) bubbling. Second, the pH of the solution was titrated to 3 with 0.2 $mol \cdot L^{-1}$ HCl and then back-titrated to 11 with 0.2 $mol \cdot L^{-1}$ NaOH. The control was performed using a blank solution without MA. During titration, the functional sites on the MA surface were occupied by metallic cations and H^+ through the following possible reactions [22]:

$$\equiv SO^- Me^{n+} + H^+ \leftrightarrow \equiv SO^- H^+ + Me^{n+} \quad (1)$$

$$\equiv SO^- H^+ + NaOH \leftrightarrow \equiv SO^- Na^+ + H_2O \quad (2)$$

where $\equiv SO^-$ represents the surface sites, such as $\equiv FeO^-$, $\equiv SiO^-$, and $\equiv AlO^-$; and Me represents the metallic cations, such as Na^+, Mg^{2+}, and Ca^{2+}.

Third, the Gran function value (G) was calculated using Eqs. (3) and (4):

$$G = (V_0 + V_1 + V_2) \times 10^{-pH}, \ pH > 7 \quad (3)$$

$$G = (V_0 + V_1 + V_2) \times 10^{-(13.8-pH)}, \ pH > 7 \quad (4)$$

where V_0, V_1, and V_2 represent the volumes (mL) of the deionized water, the titrated HCl, and the NaOH, respectively.

By drawing the Gran plot, the equivalence points V_{eb1} and V_{eb2} were calculated from the intersections of the linear portions with the G value versus the NaOH volume.

Fourth, the H_s ($mmol \cdot g^{-1}$) of the MA was calculated using the following equation:

$$H_s = \frac{(V_{eb2}^{MA} - V_{eb1}^{MA}) - (V_{eb2}^{blank} - V_{eb1}^{blank})}{m_1} \times C_{NaOH} \quad (5)$$

where C_{NaOH} represents the concentration of NaOH ($mol \cdot L^{-1}$) and m_1 represents the weight of the MA (g). The superscript MA and blank represent the test sample with the addition of MAs and the blank sample without adding MAs, respectively.

2.5. Batch adsorption experiment

Of the four MAs, MA2 demonstrated the optimal saturation magnetization (8.15 $emu \cdot g^{-1}$) and H_s (0.75 $mmol \cdot g^{-1}$), and was used for subsequent TC adsorption. 30 $mg \cdot L^{-1}$ of TC stock solution was used to investigate the effect of pH on MA2 adsorption; the pH range was from 3 to 11, and was adjusted by adding 5% HCl or 5% NaOH. 0.1 g MA2 was mixed with 20 mL stock solution in a 50 mL flask. The flask was placed in a shaker (THZ-98A, Yiheng, China) and shaken at 150 $r \cdot min^{-1}$ for 30 h at room temperature. Next, MA2 was magnetically removed from the flask and the supernatant was collected for pH and TC analysis. The adsorption capacity (q_e, $mg \cdot g^{-1}$) of the TC at equilibrium was calculated by the following equation:

$$q_e = \frac{(C_0 - C_e) \times V}{m_2} \quad (6)$$

where C_0 and C_e are the initial and the equilibrium concentrations of TC ($mg \cdot L^{-1}$), respectively; V is the solution volume (L); and m_2 is the weight of the MA2 (g).

The adsorption kinetics of TC on MA2 were investigated at pH 5 with a TC concentration of 30 $mg \cdot L^{-1}$. Equilibrium isotherm experiments were also performed at pH 5 with a TC concentration ranging from 0 to 2000 $mg \cdot L^{-1}$ and an equilibrium time of 30 h.

All adsorption experiments were conducted three times, and the experimental data were averaged.

3. Results and discussion

3.1. Fe oxide phase transformation

The transmission Mössbauer spectroscopy and XRD experiments were performed to demonstrate the phase transformation of Fe oxides in the sludge after hydrothermal treatment. As shown in Fig. 1, the XRD pattern of the sludge presented a weak peak $2\theta = 33.1°$, which belonged to hematite (JCPDS No. 33-0664). The Mössbauer spectrum of the sludge (Fig. 2(a)) showed a strong doublet and a weak sextet. The doublet exhibited an isomer shift (IS) of 0.26 $mm \cdot s^{-1}$ and an electric quadrupole splitting (QS) of 0.71 $mm \cdot s^{-1}$, and was attributed to ferrihydrite. The sextet spectrum of IS = 0.41 $mm \cdot s^{-1}$ and QS = 0.36 $mm \cdot s^{-1}$ was affiliated with hematite. After calculating the relative area of the subspectrum, the ferrihydrite content was determined to be approximately 91.2% in the Fe oxides of the sludge (Supplementary data, Table S1), indicating that it is predominant in the sludge.

With the addition of NaOH, the diffraction peak of the hematite became sharp, and a new peak appeared in the curve of MA0.6 at $2\theta = 35.6°$, which belonged to maghemite (JCPDS No. 39-1346). Accordingly, three subspectra were observed in the Mössbauer spectrum of MA0.6 (Fig. 2(b)), two of which belonged to ferrihydrite and hematite, respectively, and the third, a new subspectrum with IS = 0.32 $mm \cdot s^{-1}$ and QS = 0.23 $mm \cdot s^{-1}$, being attributed to maghemite.

With the NaOH concentration increasing from 0.6 to 4 $mol \cdot L^{-1}$, the diffraction peaks of hematite and maghemite intensified (Fig. 1). Moreover, the percentages of hematite and maghemite increased from 9.3% to 17% and from 2.1% to 13.3%, respectively, whereas the percentage of ferrihydrite steadily decreased from 88.6% to 69.7% (Supplementary data, Table S1). These results indicate that the ferrihydrite in the sludge was transformed to maghemite and hematite. Pure ferrihydrite was converted rapidly to hematite when the temperature was higher than 150 °C [23], but the transformation proceeded slowly in the presence of impurities such as Si, Al, and phosphorus (P) [23,24]. Liu et al. [25] reported

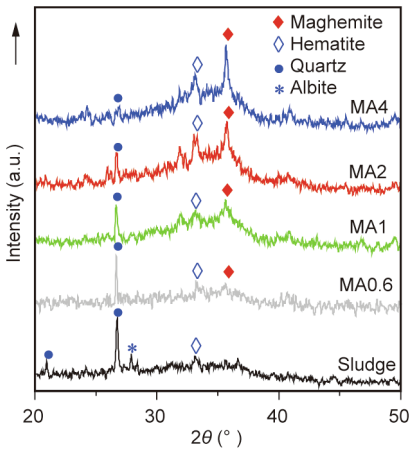

Fig. 1. XRD patterns of the sludge, MA0.6, MA1, MA2, and MA4.

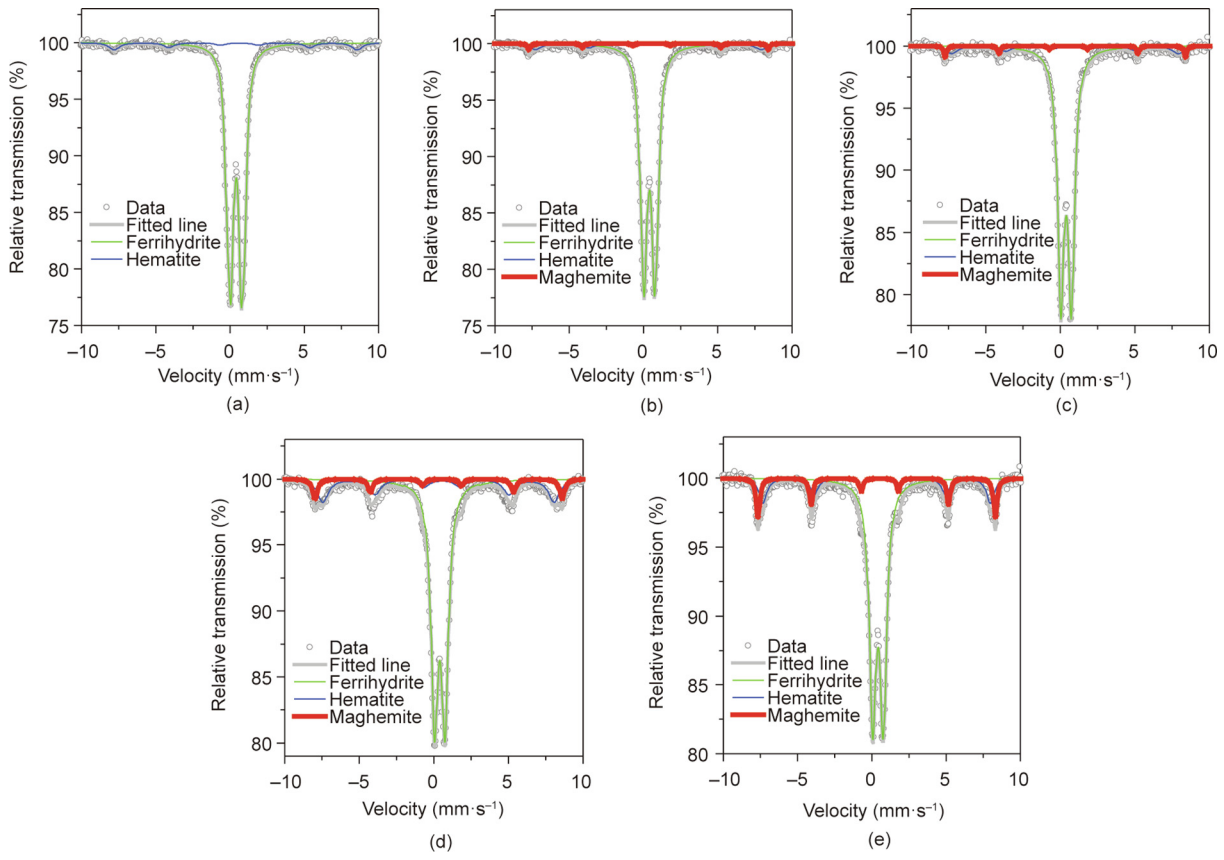

Fig. 2. Mössbauer spectrum of (a) sludge, (b) MA0.6, (c) MA1, (d) MA2, and (e) MA4.

that the product of phosphate ferrihydrite with a P/Fe ratio of 0.03 at 150 °C for 120 d was a mixture of maghemite, hematite, and residual ferrihydrite. Similar mixtures containing the same three Fe oxides were also identified with the Mössbauer spectrum in the MA (Fig. 2). Sidhu [26] reported that maghemite was completely transformed to hematite after heating at 500 °C for 3 h, and was retarded in the presence of impurities (e.g., Si and Al). Thus, in the sludge, the transformation of ferrihydrite to hematite was a two-step process, with maghemite being intermediate.

The transformation of ferrihydrite was considerably promoted by increasing NaOH concentration. With addition of NaOH, dissolution of the Si/Al oxides in the sludge occurred. As shown in Fig. 1, quartz and albite were the well-crystallized Si/Al oxides in the sludge, and these diffraction peaks gradually disappeared as the NaOH concentration increased to 4 mol·L^{-1}. These results indicated the dissolution of Si/Al oxides. The Si/Fe and Al/Fe ratios in the sludge were 0.37 and 0.09, respectively, and dropped to 0.17 and 0.04 (Fig. 3) in MA4. Accordingly, the optimal transformation of ferrihydrite was also observed in MA4 (Fig. 2 and Table S1). This phenomenon demonstrated that the loss of Si/Al impurities in the sludge promoted ferrihydrite transformation. Sludge is rich in ferrihydrite, which exists in a tetrahedrally coordinated iron structure (i.e., the iron ions are coordinated by six oxygen/hydroxyl groups) [27]. The hydroxyl groups exhibit coordinated unsaturation after dehydroxylation at high pH, thereby serving as the linkage of the small ferrihydrite particles, and allowing them to aggregate in the form of large hematite particles [28]. However, the impurities in the sludge, such as Si and Al, associate with the unsaturated sites to form an Fe–O–M (where M represents Si and Al) surface layer, which blocks the linkage of small ferrihydrite particles and inhibits ferrihydrite transformation [29]. When NaOH is introduced into the hydrothermal process, the Si/Al species with the probable forms of SiO_4^{4-} [28,30,31] and $Al(OH)_4^-$, respectively, on the unsaturated sites are replaced by OH^- via ion exchange [32]. This phenomenon results in a low ratio of Si/Fe and Al/Fe in the MA and promotes the ferrihydrite transformation.

The content of Mn in the sludge was lower than that of Si and could be coordinated to the unsaturated sites of ferrihydrite to form an Fe–O–Mn layer. Unlike the Si/Fe and Al/Fe ratios, the Mn/Fe ratio in the sludge was 0.16 and remained almost constant before and after hydrothermal treatment (Fig. 3) due to the insolubility of Mn at high pH. The valence state of Mn in the sludge and MA was characterized by XPS. As shown in Fig. 4, the spectra of the sludge had an asymmetric peak (peak A) of Mn 2p3/2 at 641.5 eV and a weak peak (peak B) at 646.3 eV, which matched well with the Mn^{4+} in MnO_2 [33] and the Mn^{2+} in the Mn–O bond

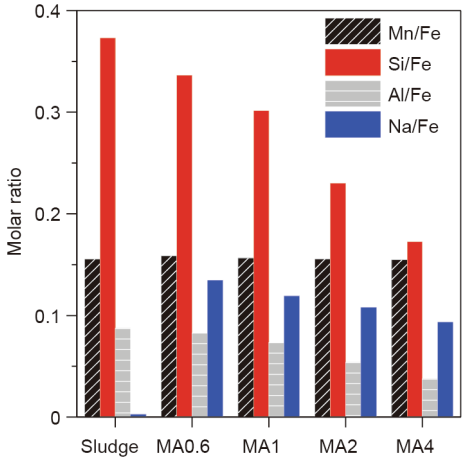

Fig. 3. Molar ratios of Mn, Si, Al, and Na to Fe in the sludge and MAs.

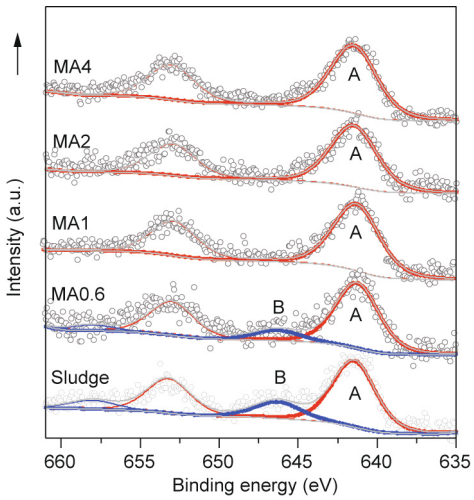

Fig. 4. High-resolution Mn 2p XPS spectrum of iron sludge and MAs.

[34], respectively. When the NaOH concentration increased to 1 mol·L^{-1}, peak B disappeared, indicating oxidization of Mn^{2+} by the dissolved oxygen in the liquid phase [35]. During Mn^{2+} oxidization, the Fe^{3+} in ferrihydrite served as an electron transporter, accepting electrons from Mn^{2+} and transferring them to oxygen (O_2) [36]. The reductive dissolution and recrystallization of ferrihydrite occurred at this stage, resulting in the formation of maghemite and hematite.

3.2. Magnetic separation

The magnetic property of the MA was significantly correlated with the percentage of maghemite in the MA. As shown in Fig. 5, a weak magnetic response was demonstrated by the sludge because no maghemite was present in it. Magnetization appeared with the hydrothermal treatment in the presence of NaOH, due to the transformation of ferrihydrite to maghemite. When the NaOH concentrations were 0.6, 1, 2, and 4 mol·L^{-1}, the saturation magnetizations of the synthesized MA were 0.43, 1.1, 8.2, and 10.9 emu·g^{-1}, respectively; this finding was in agreement with the change in the maghemite percentage (Fig. 2 and Table S1).

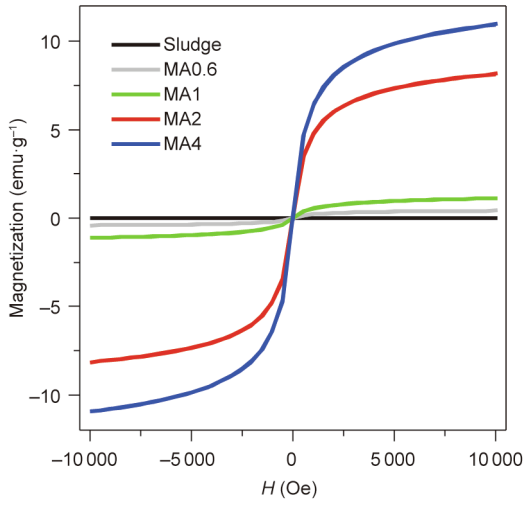

Fig. 5. Magnetic hysteresis curves of the sludge, MA0.6, MA1, MA2, and MA4. *H*: magnetic field strength. 1 Oe = 79.5775 A·m^{-1}.

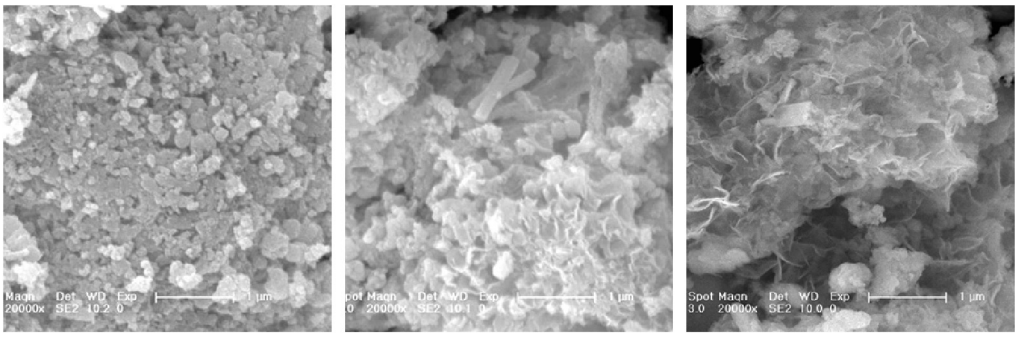

Fig. 6. SEM images of (a) the sludge, (b) MA1, and (c) MA2.

3.3. Morphology

SEM images of the sludge and MA are shown in Fig. 6. The sludge was composed of amorphous aggregates covered with small particles ranging from 200 to 500 nm in size. After hydrothermal treatment, the surface of the MA became coarse (Figs. 6(b, c)), which was attributed to the dissolution of Si/Al oxides in the presence of NaOH. The degree of roughness increased with elevation of the pH.

3.4. Adsorption

The H_s was an important parameter for estimating the adsorption property of the MA. Calculating from Fig. 7, the H_s of the MA generally declined from 1.03 mmol·g^{-1} for MA0.6 to 0.96 mmol·g^{-1} for MA1, 0.75 mmol·g^{-1} for MA2, and 0.51 mmol·g^{-1} for MA4 as the NaOH concentration increased. This decreasing trend was similar to that shown by the ferrihydrite percentage in the MA. The surface sites of the MA give it the ability to coordinate cations, such as Mg^{2+}, Ca^{2+}, and Na^{+}. In the hydrothermal process, Na^{+} was integrated into the coordination sites; thus, the Na/Fe molar ratio decreased from 0.13 for MA0.6 to 0.11 for MA2 and 0.09 for MA4 (Fig. 3), even with the increase in NaOH concentration. This decreasing trend was in agreement with the decreases in H_s and in the ferrihydrite percentage. Ferrihydrite was predominant in the sludge and had an average coordination site number of 5.4, which was higher than that of the Fe oxides (e.g., hematite) with high crystallinity [28]. Thus, phase transformation of ferrihydrite was an indicator of MA with a low H_s. Sajih et al. [37] reported that the adsorption of radium on newly generated ferrihydrite particles was nearly 100% and decreased to approximately 20% after ferrihydrite was transformed to goethite and hematite. MA2 had an H_s of 0.75 mmol·g^{-1} and a saturation magnetization of 8.2 emu·g^{-1}, indicating that MA2 is a desirable adsorbent with the property of magnetic separation.

The adsorption property of MA2 was investigated using TC as a target. Fig. 8 shows the effect of the initial pH on MA2 adsorption for TC. The removal rate of TC was approximately 87% at an initial pH below 9 and decreased to 26% at an initial pH of 11, indicating that TC adsorption on MA2 is pH dependent. When the initial pH was lower than 9, the final pH was lower than 7.4; thus, the TC was in cationic form due to the loss of protons from the phenolic diketone moiety [38]. The cationic TC could associate with the coordination sites of MA2, and an exchange between the TC and the coordinated cations (e.g., Na^{+}) occurred [39], resulting in a high removal rate of TC. When the initial pH increased to 11, the final pH increased to 8.5; in this case, the TC presented as a monovalent anion due to the loss of protons from the tricarbonyl system and the phenolic diketone moiety [38]. Therefore, the cationic exchange on the MA2 surface was interrupted, resulting in a low TC removal rate.

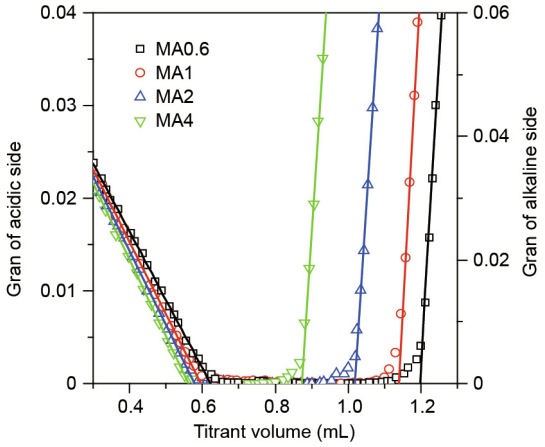

Fig. 7. Gran plots of MA0.6, MA1, MA2, and MA4.

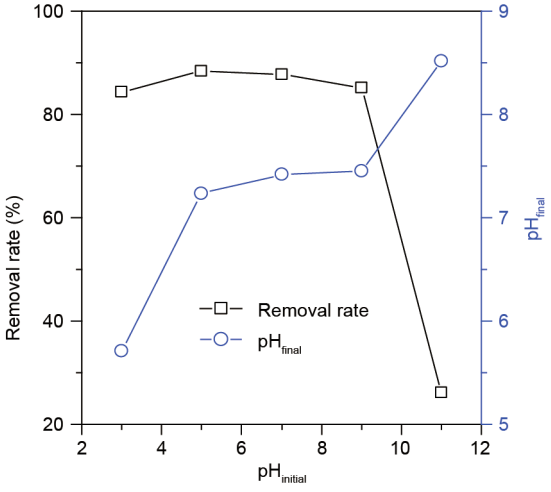

Fig. 8. The removal rate of TC and the final pH in the initial pH range of 3–11.

The adsorption kinetics of TC on MA2 were investigated, and the adsorption data was fitted with pseudo-first-order and pseudo-second-order models (Figs. 9 (a, b)). The equation of the pseudo-first-order kinetics is as follows:

$$\ln(q_e - q_t) = \ln q_e - k_1 t \quad (7)$$

where q_t is the adsorption capacity (mg·g^{-1}) of the TC at any instant time, t; and k_1 is the rate constant (L·h^{-1}) of the pseudo-first-order model.

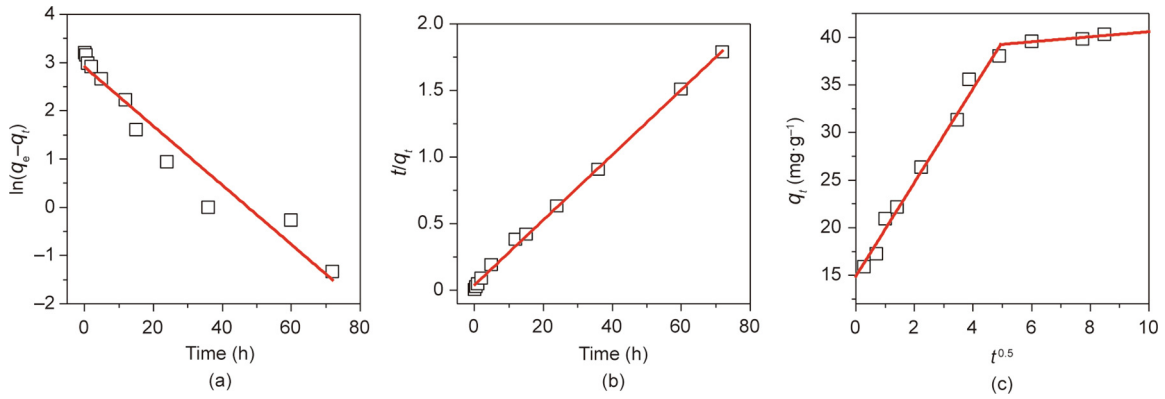

Fig. 9. Linear fitted curve of the three models for TC adsorption. (a) Pseudo-first-order kinetic model; (b) pseudo-second-order kinetic model; (c) intraparticle diffusion model.

The equation of the pseudo-second-order kinetics is as follows:

$$\frac{t}{q_t}=\frac{1}{k_2 q_e^2}+\frac{t}{q_e} \tag{8}$$

where k_2 is the rate constant ($\times 10^{-3}$ g·(mg·h)$^{-1}$) of the pseudo-second-order model.

Table 1 provides the kinetics parameters and their values of different kinetics models. The experimental q_e fitted well with the calculated value of the pseudo-second-order model, but not with that of the pseudo-first-order model. The results suggest that valence forces were involved in the exchange of electrons between TC and MA2, and that chemisorption might be the mechanism for the adsorption of TC on MA2 [40].

Weber's intraparticle diffusion model was used to analyze the adsorption data and was expressed as follows:

Table 1
Parameters and their values of the three kinetics models.

Kinetics	Parameters	Value for MA2
Pseudo-first-order kinetics	R^2	0.939
	k_1 (L·h^{-1})	0.062
	q_e (mg·g^{-1})	34.2
Pseudo-second-order kinetics	R^2	0.998
	k_2 ($\times 10^{-3}$ g·(mg·h)$^{-1}$)	0.011
	q_e (mg·g^{-1})	41.3
Intraparticle diffusion model	k_3 (mg·(g·h$^{1/2}$)$^{-1}$)	4.94
	C (mg·g^{-1})	14.87

R^2 is the regression coefficient.

$$q_t = k_3 t^{0.5} + C \tag{9}$$

where k_3 represents the intraparticle diffusion rate constant (mg·(g·h$^{1/2}$)$^{-1}$) and C represents the constant related to the boundary layer effect of the adsorption.

As shown in Fig. 9(c), Weber's model had two portions. The first portion corresponded to the gradual adsorption stage governed by intraparticle diffusion, and the second portion corresponded to the final equilibrium stage, where the intraparticle diffusion starts to slow down due to the extremely low TC concentration in the solution [41,42]. The first portion did not pass through the zero point, which indicated that the intraparticle diffusion was the rate-controlling step.

As shown in Fig. 10(a), the adsorption isotherm of the TC on MA2 was investigated. The adsorption data were analyzed using non-linear Langmuir (Eq. (10)) and Freundlich equations (Eq. (11)).

$$q_e = \frac{q_m K_L C_e}{1 + K_L C_e} \tag{10}$$

$$q_e = K_F C_e^{\frac{1}{n}} \tag{11}$$

where q_m is the maximum adsorption capacity (mg·g^{-1}), K_L is the Langmuir constant (L·mg^{-1}), K_F is the Freundlich constant (mg$^{1-1/n}$·L$^{1/n}$·g^{-1}), and n is related to the adsorption intensity [30].

Table 2 lists the parameters and their values of the Langmuir and Freundlich models. The adsorption data was in good agreement with the Langmuir model, with a high regression coefficient value (R^2) of 0.996, in comparison with the Freundlich model. The

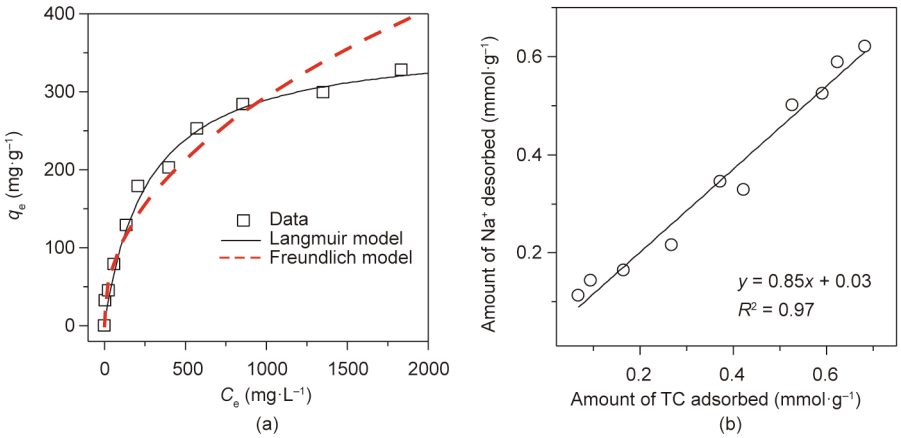

Fig. 10. (a) Adsorption isotherm of TC on MA2; (b) amount of Na^+ desorbed as affected by TC adsorption on MA2.

Table 2
Parameters and their values of the different isotherm models.

	Parameters	Value for MA2
Langmuir model	R^2	0.996
	q_m (mg·g^{-1})	362.3
	K_L (L·mg^{-1})	0.004
Freundlich model	R^2	0.958
	$1/n$	0.46
	K_F (mg$^{1-1/n}$·L$^{1/n}$·g^{-1})	11.99

results indicate that the adsorption of TC on MA2 was of a monolayer type [43,44]. The maximum capacity of MA2 for TC adsorption was 362.3 mg·g^{-1}, which was lower than those of costly carbon materials [45], but apparently higher than those of other synthesized MAs (Table 3) [45–53], such as magnetic polyacrylonitrile nanofiber mat [46], magnetic resin [47], and halloysite/$CoFe_2O_4$ composites [48]. Therefore, MA2 has great potential for TC adsorption. The amount of Na^+ desorbed from the MA2 showed a positive correlation with the amount of TC adsorbed on the MA2 (Fig. 10(b)), which confirmed that cationic exchange was the major mechanism for TC adsorption on MA2.

3.5. Environmental application

A facile hydrothermal method for the synthesis of MA was developed by treating groundwater treatment sludge, but this method is not feasible for red mud. The weakly crystallized ferrihydrite in the sludge was transformed into well-crystallized maghemite, and the prepared adsorbent had a good magnetic response. In comparison with the sludge, red mud is only rich in well-crystallized hematite and andradite [10], which need to be reductively dissolved by the addition of reductant with the formation of magnetic species [11]. A non-reductive method for MA preparation would save the disposal cost of the sludge. The MA exhibited a desirable adsorption capacity for TC and other cationic contaminants [54,55], and was reusable after regeneration under alkaline condition [56]. At the end of five cycles, the removal rate of TC was 60.9%, which was slightly lower than the 63.2% of the first round. These advantages demonstrate that the prepared MA has potential application in environment pollution control.

4. Conclusions

With alkaline hydrothermal treatment, groundwater treatment sludge comprising a mixture of ferrihydrite and other impurities (e.g., Si, Al, and Mn) was converted into MA in three steps: ① dissolution of Si/Al oxides in the sludge to the liquid fraction, ② oxidization of residual Mn^{2+} by dissolved oxygen with ferrihydrite under catalysis, and ③ promotion of the phase transformation of ferrihydrite to maghemite and hematite. The ideal MA2, synthesized with 2 mol·L^{-1} NaOH, exhibited a strong saturation magnetization of 8.2 emu·g^{-1} and a high adsorption capacity of 362.3 mg·g^{-1} for TC. Cationic exchange was the major mechanism for MA2 adsorption of TC. The results indicate that MA2 from recycled sludge is a promising adsorbent for the removal of TC from wastewater.

Acknowledgements

This work was supported by the National Natural Science Foundation of China (51578118, 51678273, 51878134, and 51878133), the Fundamental Research Funds for the Central Universities (2412017QD021) and the Science and Technology Program of Jilin Province (20190303001SF).

Compliance with ethics guidelines

Zhan Qu, Yaqiong Wu, Suiyi Zhu, Yang Yu, Mingxin Huo, Leilei Zhang, Jiakuan Yang, Dejun Bian, and Yi Wang declare that they have no conflicts of interest or financial conflicts to disclose.

Appendix A. Supplementary data

Supplementary data to this article can be found online at https://doi.org/10.1016/j.eng.2019.06.001.

References

[1] Dotremont C, Molenberghs B, Doyen W, Bielen P, Huysman K. The recovery of backwash water from sand filters by ultrafiltration. Desalination 1999;126(1):87–94.
[2] Osman SBS, Iqbal F. Possible stabilization of sludge from groundwater treatment plant using electrokinetic method. Appl Mech Mater 2014;567(419):110–5.
[3] Zhu S, Fang S, Huo M, Yu Y, Chen Y, Yang X, et al. A novel conversion of the groundwater treatment sludge to magnetic particles for the adsorption of methylene blue. J Hazard Mater 2015;292(113):173–9.
[4] Gibbons MK, Gagnon GA. Adsorption of arsenic from a Nova Scotia groundwater onto water treatment residual solids. Water Res 2010;44(19):5740–9.
[5] Zhu S, Dong G, Yu Y, Yang J, Yang W, Fan W, et al. Hydrothermal synthesis of a magnetic adsorbent from wasted iron mud for effective removal of heavy metals from smelting wastewater. Environ Sci Pollut Res Int 2018;25(23):22710–24.
[6] Liu J, Yu Y, Zhu S, Yang J, Song J, Fan W, et al. Synthesis and characterization of a magnetic adsorbent from negatively-valued iron mud for methylene blue adsorption. PLoS One 2018;13(2):e0191229.
[7] Ong DC, Pingul-Ong SMB, Kan CC, de Luna MDG. Removal of nickel ions from aqueous solutions by manganese dioxide derived from groundwater treatment sludge. J Clean Prod 2018;190:443–51.
[8] Ngatenah SNI, Kutty SRM, Isa MH. Optimization of heavy metal removal from aqueous solution using groundwater treatment plant sludge (GWTPS). In: Proceedings of the International Conference on Environment; 2010 Dec 13–15; Penang, Malaysia; 2010. p. 1–9.
[9] Yang H, Jing L, Zhang B. Recovery of iron from vanadium tailings with coal-based direct reduction followed by magnetic separation. J Hazard Mater 2011;185(2–3):1405–11.
[10] Costa RC, Moura FC, Oliveira PE, Magalhães F, Ardisson JD, Lago RM. Controlled reduction of red mud waste to produce active systems for environmental applications: heterogeneous Fenton reaction and reduction of Cr(VI). Chemosphere 2010;78(9):1116–20.

Table 3
Comparison of the adsorption capacity of TC on MA2 with other adsorbents.

Adsorbent	Raw materials	Conditions	q_m (mg·g^{-1})	Ref.
Magnetic graphene oxide sponge	Chemical reagent	pH = 3	473.0	[45]
MA2	Groundwater treatment sludge	pH = 5	362.3	This work
Fe_3O_4 incorporated polyacrylonitrile nanofiber mat	Chemical reagent	pH = 4	315.3	[46]
Magnetic resin	Chemical reagent	pH = 4	277.5	[47]
Magnetic hypercross-linked resins	Chemical reagent	pH = 4–5	214.9	[49]
Magnetic microsphere resins	Chemical reagent	pH = 6.3	166.0	[50]
Bovine serum albumin/Fe_3O_4 microspheres	Chemical reagent	pH = 5	104.3	[51]
Magnetic chitosan	Chemical reagent	pH = 5	94.3	[52]
Magnetic Fe_3O_4 resin	Resorcinol-formaldehyde resin	—	49.0	[53]
Halloysite/$CoFe_2O_4$ composites	Halloysite	pH = 5	32.2	[48]

[11] Sushil S, Alabdulrahman AM, Balakrishnan M, Batra VS, Blackley RA, Clapp J, et al. Carbon deposition and phase transformations in red mud on exposure to methane. J Hazard Mater 2010;180(1–3):409–18.
[12] Mohammed MA, Shitu A, Ibrahim A. Removal of methylene blue using low cost adsorbent: a review. Res J Chem Sci 2014;4(1):91–102.
[13] Arabi M, Ghaedi M, Ostovan A. Water compatible molecularly imprinted nanoparticles as a restricted access material for extraction of hippuric acid, a biological indicator of toluene exposure, from human urine. Microchim Acta 2017;184(3):879–87.
[14] Rajendran S, Khan MM, Gracia F, Qin J, Gupta VK, Arumainathan S. Ce^{3+}-ion-induced visible-light photocatalytic degradation and electrochemical activity of ZnO/CeO_2 nanocomposite. Sci Rep 2016;6(1):31641.
[15] Saravanan R, Karthikeyan S, Gupta VK, Sekaran G, Narayanan V, Stephen A. Enhanced photocatalytic activity of ZnO/CuO nanocomposite for the degradation of textile dye on visible light illumination. Mater Sci Eng C 2013;33(1):91–8.
[16] Ghaedi M, Hajjati S, Mahmudi Z, Tyagi I, Agarwal S, Maity A, et al. Modeling of competitive ultrasonic assisted removal of the dyes—methylene blue and safranin-O using Fe_3O_4 nanoparticles. Chem Eng J 2015;268:28–37.
[17] Ostovan A, Ghaedi M, Arabi M. Fabrication of water-compatible superparamagnetic molecularly imprinted biopolymer for clean separation of baclofen from bio-fluid samples: a mild and green approach. Talanta 2018;179:760–8.
[18] Arabi M, Ghaedi M, Ostovan A. Development of a lower toxic approach based on green synthesis of water-compatible molecularly imprinted nanoparticles for the extraction of hydrochlorothiazide from human urine. ACS Sustain Chem Eng 2017;5(5):3775–85.
[19] Ostovan A, Ghaedi M, Arabi M, Yang Q, Li J, Chen L. Hydrophilic multitemplate molecularly imprinted biopolymers based on a green synthesis strategy for determination of B-family vitamins. ACS Appl Mater Interfaces 2018;10(4):4140–50.
[20] Gupta VK, Atar N, Yola ML, Üstündağ Z, Uzun L. A novel magnetic Fe@Au core–shell nanoparticles anchored graphene oxide recyclable nanocatalyst for the reduction of nitrophenol compounds. Water Res 2014;48:210–7.
[21] Sandroni V, Smith CMM. Microwave digestion of sludge, soil and sediment samples for metal analysis by inductively coupled plasma–atomic emission spectrometry. Anal Chim Acta 2002;468(2):335–44.
[22] Duquette M, Hendershot W. Soil surface charge evaluation by back-titration: I. Theory and method development. Soil Sci Soc Am J 1993;57(5):1222–8.
[23] Barrón V, Torrent J, de Grave E. Hydromaghemite, an intermediate in the hydrothermal transformation of 2-line ferrihydrite into hematite. Am Mineral 2003;88(11–12):1679–88.
[24] Cornell RM. Effect of silicate species on the transformation of ferrihydrite into goethite and hematite in alkaline media. Clays Clay Miner 1987;35(1):21–8.
[25] Liu Q, Barrón V, Torrent J, Eeckhout SG, Deng C. Magnetism of intermediate hydromaghemite in the transformation of 2-line ferrihydrite into hematite and its paleoenvironmental implications. J Geophys Res 2008;113(B1):B01103.
[26] Sidhu PS. Transformation of trace element-substituted maghemite to hematite. Clays Clay Miner 1988;36(1):31–8.
[27] Zhao J, Huggins FE, Feng Z, Lu FL, Shah N, Huffman GP. Structure of a nanophase iron oxide catalyst. J Catal 1993;143(2):499–509.
[28] Jianmin Z. Ferrihydrite: surface structure and its effects on phase transformation. Clays Clay Miner 1994;42(6):737–46.
[29] Brinza L, Vu HP, Shaw S, Mosselmans JFW, Benning LG. Effect of Mo and V on the hydrothermal crystallization of hematite from ferrihydrite: an *in situ* energy dispersive X-ray diffraction and X-ray absorption spectroscopy study. Cryst Growth Des 2015;15(10):4768–80.
[30] Ostovan A, Ghaedi M, Arabi M, Asfaram A. Hollow porous molecularly imprinted polymer for highly selective clean-up followed by influential preconcentration of ultra-trace glibenclamide from bio-fluid. J Chromatogr A 2017;1520:65–74.
[31] Arabi M, Ghaedi M, Ostovan A. Development of dummy molecularly imprinted based on functionalized silica nanoparticles for determination of acrylamide in processed food by matrix solid phase dispersion. Food Chem 2016;210:78–84.
[32] Arabi M, Ghaedi M, Ostovan A. Synthesis and application of *in-situ* molecularly imprinted silica monolithic in pipette-tip solid-phase microextraction for the separation and determination of gallic acid in orange juice samples. J Chromatogr B Analyt Technol Biomed Life Sci 2017;1048:102–10.
[33] Militello MC, Gaarenstroom SW. Manganese dioxide (MnO_2) by XPS. Surf Sci Spectra 2001;8(3):200–6.
[34] Saravanan R, Gupta VK, Narayanan V, Stephen A. Visible light degradation of textile effluent using novel catalyst ZnO/γ-Mn_2O_3. J Taiwan Inst Chem E 2014;45(4):1910–7.
[35] Saravanan R, Khan MM, Gupta VK, Mosquera E, Gracia F, Narayanan V, et al. ZnO/Ag/Mn_2O_3 nanocomposite for visible light-induced industrial textile effluent degradation, uric acid and ascorbic acid sensing and antimicrobial activity. RSC Adv 2015;5(44):34645–51.
[36] Lan S, Wang X, Xiang Q, Yin H, Tan W, Qiu G, et al. Mechanisms of Mn(II) catalytic oxidation on ferrihydrite surfaces and the formation of manganese (oxyhydr)oxides. Geochim Cosmochim Acta 2017;211:79–96.
[37] Sajih M, Bryan ND, Livens FR, Vaughan DJ, Descostes M, Phrommavanh V, et al. Adsorption of radium and barium on goethite and ferrihydrite: a kinetic and surface complexation modelling study. Geochim Cosmochim Acta 2014;146:150–63.
[38] Kulshrestha P, Giese Jr RF, Aga DS. Investigating the molecular interactions of oxytetracycline in clay and organic matter: insights on factors affecting its mobility in soil. Environ Sci Technol 2004;38(15):4097–105.
[39] Saravanan R, Sacari E, Gracia F, Khan MM, Mosquera E, Gupta VK. Conducting PANI stimulated ZnO system for visible light photocatalytic degradation of coloured dyes. J Mol Liq 2016;221:1029–33.
[40] Ho YS, McKay G. Pseudo-second order model for sorption processes. Process Biochem 1999;34(5):451–65.
[41] Gupta VK, Saleh TA. Sorption of pollutants by porous carbon, carbon nanotubes and fullerene—an overview. Environ Sci Pollut Res Int 2013;20(5):2828–43.
[42] Gupta VK, Nayak A, Agarwal S, Tyagi I. Potential of activated carbon from waste rubber tire for the adsorption of phenolics: effect of pre-treatment conditions. J Colloid Interface Sci 2014;417:420–30.
[43] Mittal A, Mittal J, Malviya A, Gupta VK. Removal and recovery of chrysoidine Y from aqueous solutions by waste materials. J Colloid Interface Sci 2010;344(2):497–507.
[44] Saleh TA, Gupta VK. Photo-catalyzed degradation of hazardous dye methyl orange by use of a composite catalyst consisting of multi-walled carbon nanotubes and titanium dioxide. J Colloid Interface Sci 2012;371(1):101–6.
[45] Yu B, Bai Y, Ming Z, Yang H, Chen L, Hu X, et al. Adsorption behaviors of tetracycline on magnetic graphene oxide sponge. Mater Chem Phys 2017;198:283–90.
[46] Liu Q, Zheng Y, Zhong L, Cheng X. Removal of tetracycline from aqueous solution by a Fe_3O_4 incorporated PAN electrospun nanofiber mat. J Environ Sci 2015;28:29–36.
[47] Zhou Q, Li Z, Shuang C, Li A, Zhang M, Wang M. Efficient removal of tetracycline by reusable magnetic microspheres with a high surface area. Chem Eng J 2012;210:350–6.
[48] Guan W, Wang X, Pan J, Lei J, Zhou Y, Lu C, et al. Synthesis of magnetic halloysite composites for the effective removal of tetracycline hydrochloride from aqueous solutions. Adsorpt Sci Technol 2012;30(7):579–91.
[49] Zhang M, Li A, Zhou Q, Shuang C, Zhou W, Wang M. Effect of pore size distribution on tetracycline adsorption using magnetic hypercrosslinked resins. Micropor Mesopor Mat 2014;184:105–11.
[50] Li B, Ma J, Zhou L, Qiu Y. Magnetic microsphere to remove tetracycline from water: adsorption, H_2O_2 oxidation and regeneration. Chem Eng J 2017;330:191–201.
[51] Zhang B, Zhang H, Li X, Lei X, Li C, Yin D, et al. Synthesis of BSA/Fe_3O_4 magnetic composite microspheres for adsorption of antibiotics. Mater Sci Eng C 2013;33(7):4401–8.
[52] Raeiatbina P, Açıkelb YS. Removal of tetracycline by magnetic chitosan nanoparticles from medical wastewaters. Desalination 2017;73:380–8.
[53] Yan X, Gan K, Tian B, Zhang J, Wang L, Lu D. Photo-fenton refreshable Fe_3O_4@HCS adsorbent for the elimination of tetracycline hydrochloride. Res Chem Intermed 2018;44(1):1–11.
[54] Khani H, Rofouei MK, Arab P, Gupta VK, Vafaei Z. Multi-walled carbon nanotubes-ionic liquid-carbon paste electrode as a super selectivity sensor: application to potentiometric monitoring of mercury ion(II). J Hazard Mater 2010;183(1–3):402–9.
[55] Gupta VK, Nayak A, Agarwal S. Bioadsorbents for remediation of heavy metals: current status and their future prospects. Environ Eng Res 2015;20(1):1–18.
[56] Gupta VK, Jain R, Nayak A, Agarwal S, Shrivastava M. Removal of the hazardous dye—tartrazine by photodegradation on titanium dioxide surface. Mat Sci Eng C Mater 2011;31(5):1062–7.